

First-principles calculation of the TiN effective work function on SiO₂ and on HfO₂

L. R. C. Fonseca*

Wernher von Braun Center for Advanced Research, Avenida Perimetral Norte 301, Campinas, São Paulo 13098-381, Brazil

A. A. Knizhnik†

Kinetic Technologies Ltd., Kurtchatov Square 1, Moscow 123182, Russia

(Received 23 June 2006; revised manuscript received 1 September 2006; published 3 November 2006)

This paper reports density functional theory (DFT) electronic structure calculations of the valence band offsets (VBO) between TiN and cristobalite SiO₂ and between TiN and monoclinic HfO₂ for various interface chemical compositions. To investigate the impact of species interdiffusion on the effective TiN work function, we considered modifications of the TiN and dielectrics composition within the first monolayer from the interface. We found that the calculated VBO's depend on the stoichiometry of the interface: they are the smallest for oxygen/nitrogen rich interfaces and increase for reduced interfaces where metal-metal bonds are formed. The impact of the interface stoichiometry on the VBO for the assumed interface models can be as large as 0.3 eV and 1.2 eV for the TiN/SiO₂ and TiN/m-HfO₂ interfaces, respectively. We also found that species interdiffusion within our model systems does not affect the VBO significantly. All the calculated VBO's obtained from stoichiometric interfaces and their structural modifications are smaller than expected from available data. Finally we considered possible schemes for calculating the effective metal work function on a dielectric. We conclude that the rather poor accuracy of such work function calculations (stemming from the underestimated VBO's) may be explained by the crudeness of our model interface, which is limited by the lack of experimental data on the interfaces atomistic structures. Our analysis indicates that with the introduction of a transition region between the metal and the dielectric instead of the sharp interfaces and their slight variations studied here, or by overoxidizing the interface, the calculated VBO's may improve. On the other hand, the accuracy problem may have a more fundamental origin, namely the local density approximation (LDA) of DFT which leads to a severe band gap underestimation. Scaling our calculated VBO's by the corresponding experimental band gaps yields better agreement with measured TiN work functions on HfO₂ for stoichiometric or near-stoichiometric interfaces. However, for TiN on SiO₂ the scaled VBO is still considerably smaller than experimental data suggests. The inclusion of *GW* corrections or self-interaction corrected pseudopotentials improves the agreement with experimental data significantly, which strongly suggests that the VBO is underestimated by LDA/DFT as well as the band gap.

DOI: [10.1103/PhysRevB.74.195304](https://doi.org/10.1103/PhysRevB.74.195304)

PACS number(s): 73.20.-r, 73.30.+y, 71.15.Mb, 85.30.De

I. INTRODUCTION

The stringent sub-1 nm equivalent oxide thickness (EOT) and low-leakage current requirements for advanced complementary metal oxide semiconductor (CMOS) technology as prescribed by the International Technology Roadmap for Semiconductors (ITRS) (Ref. 1) have forced the semiconductor industry to consider the replacement of two key materials used in CMOS at once: SiO₂ by a high-permissivity (high-*K*) dielectric, and polysilicon (poly-Si) by a metal gate. The need for a metal gate stems from the fact that despite the reduced leakage current measured for several high-*K* dielectrics with respect to SiO₂ for the same EOT, poly-Si depletion severely limits EOT scaling.² Thin film amorphous or polycrystalline HfO₂ has a relatively high dielectric constant (15–20) and is reasonably stable in contact with silicon and poly-Si (a 5–15 Å thick SiO₂-rich interfacial layer is usually formed between HfO₂ and the Si substrate) and with a number of metals.^{3,4} Thus HfO₂ has become a serious contender for SiO₂ replacement. TiN, on the other hand, is a midgap metal with a work function (*WF*) of ~4.7 eV from capacitance-voltage (*CV*) measurements on SiO₂,⁴ which precludes its direct use as a metal gate for bulk CMOS application. Even though research has revealed that the TiN *WF* can

be modulated within the range 4.8–5.3 eV,⁵ its dependence on the annealing temperature makes it less suitable.⁶ Nevertheless, due to its stability and compatibility with industrial deposition and processing techniques, TiN is normally used to benchmark the physical properties of high-*K* dielectrics. It may also be used as a gate metal for silicon on insulator (SOI), which is more flexible concerning the alignment between the metal Fermi level and the Si substrate band edges.² Therefore, the TiN/HfO₂ stack is an important model system for theoretical investigation. We believe that the knowledge gained from the study of this system can be readily transferred to similar metal/oxide stacks.

A serious issue in the path for high-*K* dielectrics introduction in new products is the need to achieve low-threshold voltage (*V_t*; see Fig. 1 for notation and definitions used throughout the text), which is the required bias applied to the metal gate to turn the transistor on. Low *V_t* values are highly desirable for low power consumption and high on/off switching speeds. The requirement to achieve low *V_t*'s is that the metal Fermi level nearly aligns with the Si band edges, the conduction/valence band edge (CBE/VBE) in the *n*-type metal-oxide semiconductor (NMOS) and *p*-type metal-oxide semiconductor (PMOS) cases (in NMOS/PMOS, the channel is doped with holes/electrons while the inversion well formed at the substrate/dielectric interface carries electrons/

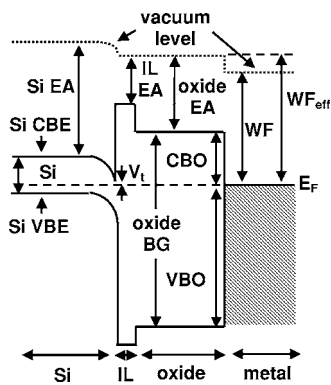


FIG. 1. Notation and definitions used in the text. CBE: conduction band edge; VBE: valence band edge; IL: interfacial layer; EA: electron affinity; V_t : threshold voltage; BG: band gap; CBO: conduction band offset; VBO: valence band offset; WF: vacuum work function; WF_{eff} : effective work function; E_F : Fermi level. The vacuum level step at the oxide/metal interface is due to charge transfer across the interface (see text for detailed discussion). The VBO and CBO are only indicated for the metal/oxide interface; however they can also be seen for the Si/IL and IL/oxide interfaces.

holes from source to drain). The Si/SiO₂/poly-Si stack is convenient because the substrate/poly-Si Fermi levels can be tuned by just doping with either electron donor or electron acceptor species. In the case of a metal gate, many suggestions have been made in recent years to use a single metal for NMOS and PMOS through modulation of the metal WF by metal alloying⁷ and species implantation.⁸ However, despite the considerable advantage of this procedure in terms of reducing the number of deposition/etch steps and thus process complexity and cost, to our best knowledge none of those ideas have yet achieved the desired WF values. Therefore, two distinct metals may be necessary to replace poly-Si and yield the required low V_t in bulk CMOS.

If there is no charge transfer at the metal/dielectric interface, the so-called weak Fermi pinning limit or Schottky limit, poly-Si could be simply replaced by two metals with vacuum WF's of 4.1 ± 0.1 eV and 5.1 ± 0.1 eV for NMOS and PMOS, respectively.⁹ On the other hand, in the so-called strong pinning limit or Bardeen limit, the amount of charge transferred across the interface is such that the metal/dielectric valence band offset (VBO) is always the same, independently of the metal vacuum WF. High- K dielectrics of interest, such as HfO₂ (and corresponding silicate and aluminate) and Al₂O₃, are expected to pin at an intermediate level, between the Schottky and Bardeen limits.¹⁰ Fermi level pinning causes the formation of an interface dipole and corresponding vacuum level discontinuity at the interface [Fig. 2; band offsets from Ref. 11 and electron affinities (EA) from Refs. 10 and 12 assuming that the interfacial layer (IL) SiO_x EA is the same as of SiO₂]. As a result, the location of the metal Fermi level with respect to the substrate and dielectric band edges (or effective work function, WF_{eff}) changes from its unpinned (Schottky) location causing the substrate bands to bend. Uncontrolled substrate band bending impacts the electrical characteristics of the device driving it to suboptimal operation.⁹ Therefore it is of great interest to theoretically predict with accuracy better than ± 100 meV by

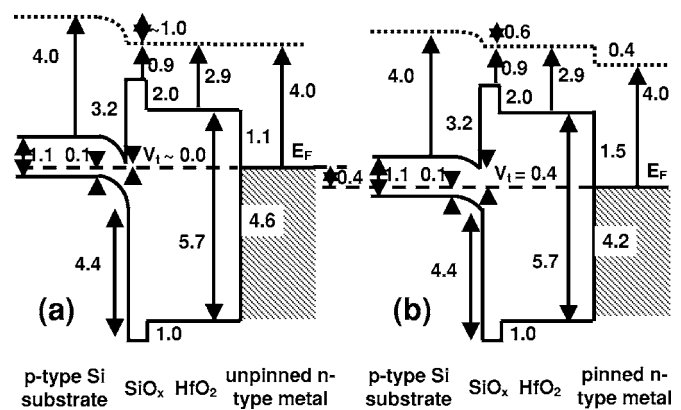


FIG. 2. Band diagram for a gate stack composed of Si/SiO_x/HfO₂/metal, where the fictitious metal vacuum work function is 4.0 eV. The Si, SiO_x, and HfO₂ band gaps/electronegativities are, respectively, 1.1/4.0, 0.9/8.7, and 5.7/2.9 eV. In this example we assume that the SiO_x layer has electrical parameters similar to SiO₂. The Si/SiO_x band offsets were taken from Ref. 11 and electron affinities from Refs. 10 and 12. (a) No charge transfer takes place across the interface, thus no Fermi pinning occurs. In this case the metal vacuum work function coincides with its effective work function [$=\text{CBO}(\text{ox}/\text{metal})+\text{EA}(\text{ox})=1.1 \text{ eV}+2.9 \text{ eV}=4.0 \text{ eV}$]. Because the Si substrate is p doped and the metal work function aligns with the Si CBE, the substrate band bends by approximately 1 eV, as indicated by the voltage drop in the vacuum level (dashed line). The resulting threshold voltage is very small. (b) Charge has transferred from the metal to the HfO₂ layer, increasing the Schottky barrier by 0.4 eV (as an example). The effective metal work function is 4.4 eV and does not coincide with its vacuum work function. Since the effective work function has shifted towards the Si midgap, the Si band bending is less and the threshold voltage increases to ~ 0.4 eV. The voltage drop takes place in the Si substrate (0.6 eV) and at the dielectric/metal interface (0.4 eV).

how much a given metal WF_{eff} differs from its vacuum WF, thus avoiding expensive and time consuming experimental evaluations of candidate metal gates. WF_{eff} is simply given by the metal-dielectric conduction band offset (CBO) plus the dielectric EA if there are no other dipoles in the gate stack. Without interface pinning, which affects the CBO, WF_{eff} coincides with the vacuum WF [Fig. 2(a)]. Pinning is known to occur at both metal/HfO₂ and Si/HfO₂ interfaces;^{13,14} however, in all practical device implementations of HfO₂ on Si, the Si substrate is separated from HfO₂ by an IL sometimes consisting of graded SiO_x, usually 5–15 Å thick, with x increasing from 0 at the interface with the substrate to <1 at the interface with the dielectric, plus perhaps small amounts of Hf.¹⁵ Since SiO₂ is a weak Fermi level pinner,^{10,13} in this work we assume that the SiO_x IL works as a buffer, thus avoiding the pinning of the substrate. Therefore we neglect any pinning at the interface between silicon and HfO₂ and only consider pinning at the dielectric/metal interface. While WF_{eff} is a measure of the alignment between the metal Fermi level and the dielectric band edges, under this assumption it is also a measure of the alignment between the metal Fermi level and the Fermi level of the substrate [Fig. 2(b)]. Low V_t 's are obtained if the WF_{eff} 's of the metal replacements are within ± 100 meV of the n - and p -doped substrate Fermi levels.

In this work we investigate crystalline TiN/SiO₂ and TiN/HfO₂ model systems to gain insight on the relation between interface atomic configurations, including O vacancies, and the VBO. Because SiO₂ is a weak pinner, the TiN WF and WF_{eff} in this case should be similar. Thus, TiN/SiO₂ is included as a standard against which the TiN/HfO₂ results can be compared, and to validate the approach used in this work. Even though SiO₂ is amorphous and HfO₂ is at least partially amorphous before high temperature anneal, our crystalline model should still provide helpful general trends, especially because at the small atomic length scale that sets the VBO, real amorphous interfaces can be approximated as the average of a set of locally crystalline interfaces. We investigate the impact on VBO of species migration across the interface, since that is likely to happen either upon metal deposition or during post-deposition temperature annealing. Bulk and interface charges created by charge exchange between the substrate/metal gate and trap centers in the dielectric can also affect V_t . Here we do not consider the case of net charged dielectrics or extended dipoles leading to long range band bending but only the effect of local dipoles on V_t . Finally we discuss possible schemes to calculate WF_{eff} and suggest that their accuracy is limited by our poor experimental knowledge of the atomic structure of dielectric/metal interfaces. We also suggest that the underestimation of the band gap using the local density approximation [LDA (Refs. 16 and 17)] of DFT may set a fundamental limit to the accuracy of such calculations.

II. METHOD

A. Semiempirical techniques for valence band offset estimation

Among the many Fermi pinning models developed to understand and predict metal/dielectric VBO's,¹⁸⁻²¹ the metal-induced gap states (MIGS) model^{20,21} in its most phenomenological formulation¹⁰ has been extensively used for predictions of interface VBO's due to its considerable level of success¹³ and because it offers a simple scheme to predict Schottky barriers from the knowledge of bulk dielectric parameters only, without the need of involved interface calculations.

As a metal comes in contact with the dielectric surface, the metal wave functions leak into the dielectric, inducing gap states. The MIGS are loosely related to the exponentially decaying gap states in the bulk dielectric, which are only meaningful near the surface. The MIGS's transition from valence to conduction band character (determined by the branch point of smallest decay rate in the complex band structure of the bulk dielectric²⁰) suggests the location of the highest occupied gap state, or charge neutrality level (φ_{CNL}). On the other hand, surface states of a dielectric originate from the broken chemical bonds and defects created as a bulk dielectric is cut in order to expose a surface. The MIGS model neglects the pinning effect of broken bonds and interface defects and assumes that the MIGS are solely responsible for the metal Fermi level pinning. In this case, to predict band offsets the MIGS model only requires the knowledge of two quantities, the location of φ_{CNL} and the

pinning strength S , which is a measure of the dielectric Fermi pinning strength. In this approximation the metal/dielectric WF_{eff} is given by

$$WF_{eff} = S(WF - \varphi_{CNL}) + \varphi_{CNL}, \quad (1)$$

where the pinning strength S can be estimated quite accurately using the approximate formula²²

$$S = \frac{1}{1 + 0.1(\epsilon_{\infty} - 1)^2}. \quad (2)$$

The location of φ_{CNL} can be calculated following Tersoff's proposed method to locate the branch point by calculating the zero of the Green's function along a judiciously chosen crystallographic direction.²¹ Later Robertson proposed a simpler formula,¹⁰ which is appropriate for a tight-binding model calculation since the energy spectrum has an upper bound; however, in principle it is divergent. Complex band structure calculations of bulk dielectrics provide a systematic approach for locating φ_{CNL} as shown by Demkov *et al.*,²³ despite the uncertainty created by the large DFT/LDA band gap underestimation.

Therefore, the MIGS framework provides a convenient means for estimation of Schottky barriers based on bulk properties of the dielectric without considering the interface in atomic detail.

Previous studies of Fermi pinning in Si/HfO₂/poly-Si show that for typical dielectric and poly-Si deposition techniques, the pinning strength of HfO₂ is considerably higher than what the MIGS model predicts.^{10,14} Moreover, it has been shown that the high V_t measured for Si/HfO₂/poly-Si and Si/Al₂O₃/poly-Si systems is caused by Fermi pinning at the dielectric/poly-Si interface and may be related to oxygen-deficient interfaces.¹⁴ Therefore it is reasonable to expect that in addition to MIGS, surface states, which can only be investigated at the atomic level, also play a relevant role in the Fermi pinning of high- K dielectrics.²²

B. Electronic structure calculation

Calculations were performed using the generalized gradient approximation (GGA) (Ref. 24) within DFT (Refs. 25 and 26) as implemented in the local orbital SIESTA code.²⁷ Norm-conserving nonlocal pseudopotentials (PP's) of the Troullier-Martins type were used to describe all the elements.²⁸ The atomic configuration [Kr 4d¹⁰4f¹⁴5s²5p⁶]5d²6s² was used for the Hf PP and [Ar]3d²4s² for the Ti PP. Semicore corrections were used for both elements. Negligible (less than 100 meV) impact on the calculated VBO was found with the inclusion of the 5p⁶ and 3p⁶ states in the Hf and Ti PP's, respectively. A set of two special k -points in the plane parallel to the TiN/dielectric interfaces (xy plane) were used for the Brillouin zone integration during relaxation, and 12 k -points were used for the subsequent density of states calculation.²⁹ Relaxation using three and six k -points in the plane changed the calculated VBO's by less than 50 meV for both TiN/SiO₂ and TiN/HfO₂ interfaces. The model structures calculated were

of the type TiN(111)/dielectric, with four Ti/N intercalated layers forming a slab ~ 10 Å thick. The VBO's changed by less than 100 meV for thicker metal slabs. Crystobalite SiO₂ and monoclinic (001) HfO₂ slabs ~ 13.7 Å and ~ 10.2 Å thick, respectively, were used. As will be discussed later, those dielectric slab thicknesses were not enough to fully exclude interface properties in the density of state (DOS) taken at the furthest point from the interface with the metal. Nevertheless the accuracy of the results is enough to reach semiquantitative conclusions and to indicate trends.

Periodic boundary conditions were applied along the x and y directions parallel to the plane of the interface. The length of the unit cell vectors in the xy plane were obtained from bulk relaxation of the unit cell vectors of the respective dielectrics. In order to fit the HfO₂ and SiO₂ planar cell size, the TiN slabs were stretched along the interface plane. As we will see later the lattice mismatch in the plane for both interfaces is not so significant, thus the corresponding compression along the z direction is minor and was not considered in the double interface cases, which are explained below. Calculations including a vacuum gap produced essentially the same VBO for the TiN/SiO₂ case (see below), indicating that indeed the TiN lattice adjustment along z is not important in this case. On the other hand, calculations of the TiN/HfO₂ interface with a vacuum gap resulted in a VBO ~ 0.3 eV smaller than for the double interface case, which we attribute from PDOS analysis (not shown) to residual HfO₂ surface states not fully saturated by hydrogen. The lattice vectors misfit was improved by matching five TiN(111) cells in the [100] direction (15.13×5.24 Å²) to three SiO₂ (16.08×5.36 Å²) and to three HfO₂ (15.78×5.29 Å²) cells, resulting in a maximum calculated lattice mismatch of $\sim 6\%$ for SiO₂ and $\sim 4\%$ for HfO₂. To assess the impact of stressing the metal slab on its WF we calculated the vacuum WF of stressed TiN using the same lattice cell vectors in the xy plane as in the interface calculations, and without stress using optimized cell vectors for TiN. Those calculations gave 4.7 eV for the fully relaxed case, while using the HfO₂/SiO₂ lattice vectors the WF 's are 4.6/4.5 eV, respectively. Thus stress is most likely not a big factor in this study. Along the z directions two cases were considered: a periodic structure with and without a vacuum gap. In the case of a vacuum gap the TiN and HfO₂ (SiO₂) layers were terminated at a Ti and a Hf (Si) plane and saturated with hydrogen atoms. While the vacuum gap allows for relaxation along the z direction to eliminate any residual stresses, it may be difficult to properly saturate all the dangling bonds in the dielectric side, especially in the case of HfO₂. Moreover, the presence of a vacuum gap introduces a slab to slab net dipole due to the different exposed surfaces. The resulting electric field creates a potential drop in the dielectric which makes it difficult to determine the VBO using the method of van de Walle and Martin³⁰ described below. The VBO obtained in the presence of the vacuum gap is less than 200 meV larger than without a vacuum gap for TiN/HfO₂ and is the same for TiN/SiO₂ in the case of stoichiometric interfaces. For the nonstoichiometric interface structures, only the double interface models (no vacuum gap) were used to calculate the VBO.

All calculations were performed using SIESTA's most

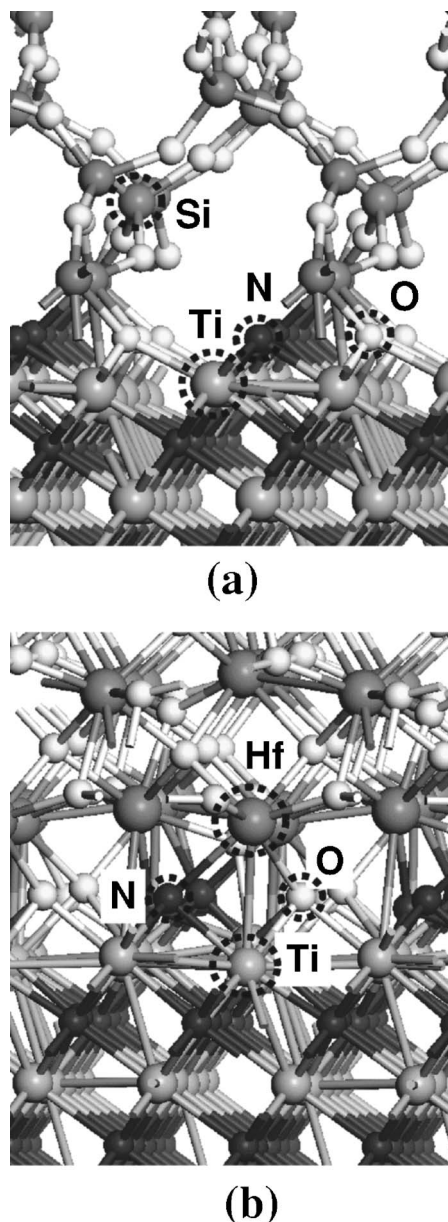


FIG. 3. Relaxed reference (a) TiN/SiO₂ and (b) TiN/HfO₂ interfaces. Notice the alternating O and N rows along the interfaces that maintain the stoichiometry of the metal and dielectrics. The remaining interfaces considered in this work result from variations of interfaces (a) and (b).

accurate basis set [double- ζ plus polarization (DZP)]. The other basis sets available in Siesta are the single- ζ (SZ), double- ζ (DZ), and the single- ζ plus polarization (SZP). The HfO₂ band gaps calculated using SZ, SZP, DZ, and DZP, are respectively 3.17 eV, 3.59 eV, 3.75 eV, and 3.86 eV.²⁷

The reference TiN/dielectric interfaces were obtained by adding O and N between a Ti and a Hf (Si) layer to keep the appropriate stoichiometry. Figure 3 shows the interface details of the relaxed structures. To this date there is no experimental characterization of the TiN/HfO₂ and TiN/SiO₂ interfaces structures at the atomic level. Therefore, our choice of atomic configuration is largely arbitrary and aims to provide trends only.

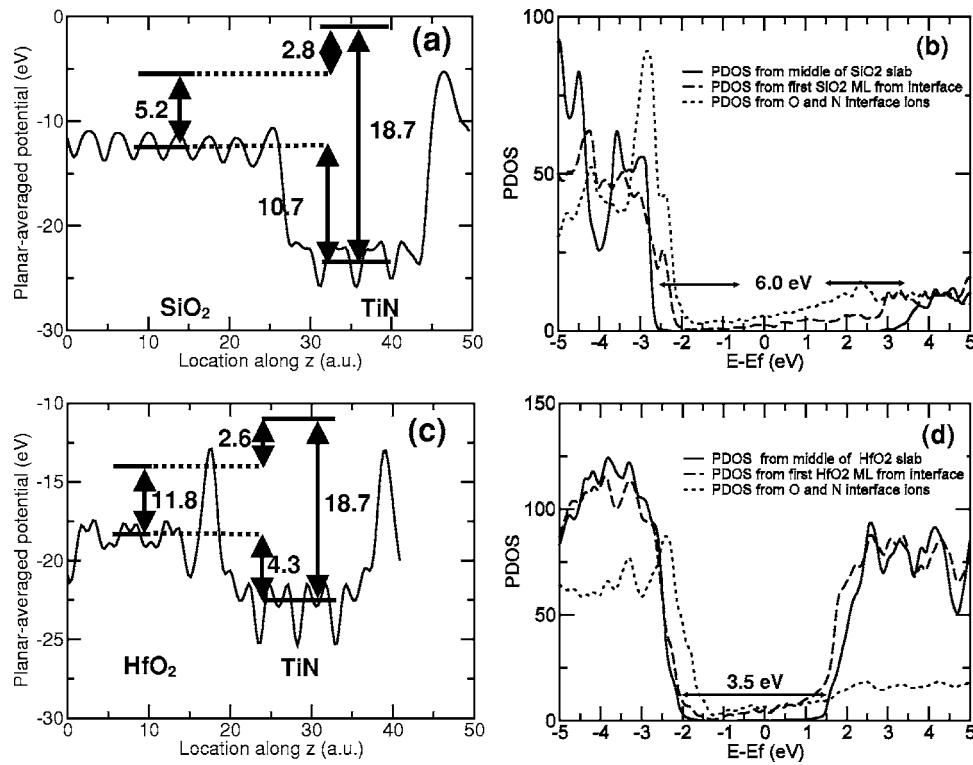


FIG. 4. (a) and (c) Planar-averaged potentials of the TiN/SiO₂ and TiN/HfO₂, respectively, using the stoichiometric interfaces of Fig. 3. Averages along the z direction (horizontal bars on wiggled lines) are taken in narrow regions at the center of the slabs. Valence band edges (horizontal bars above wiggled lines) are obtained by shifting (vertical arrows) the average potential by an amount μ obtained from bulk calculations of the metal and dielectric according to the method of van de Walle and Martin (Ref. 30). The resulting VBO's are 3.4 eV for TiN/SiO₂ and 3.0 eV for TiN/HfO₂ interfaces. (b) and (d) PDOS of TiN/SiO₂ and TiN/HfO₂ interfaces, respectively, using a Gaussian smearing of 100 meV. Solid lines: DOS projected on Si (Hf) and O atoms at the middle of the dielectric slab; dashed lines: DOS projected on the first SiO₂ (HfO₂) monolayer away from the interface; dotted lines: DOS projected on the interfacial O and N atoms plus the first plane of Si (Hf) atoms away from the interface. Arrows indicate the approximate locations of the valence and conduction band edges and the corresponding band gaps for the solid lines. All values are in eV.

C. Valence band offset calculation

Two techniques were used to determine the VBO between TiN and the dielectrics using the results of the first principles calculations: the method of van de Walle and Martin (WM) (Ref. 30) and analysis of the density of states projected on planes of atoms (PDOS) away from the interface. In the WM method, the VBO results from the difference between the vacuum energy and the shifted planar-averaged total potential in each region. The shift is obtained for each material as the difference between the bulk Fermi level and the bulk planar-averaged potential obtained from separate bulk calculations (using relaxed lattice vectors for the dielectrics, but stressed lattice vectors for the metal). This recipe can be simplified somewhat by taking directly the difference between the slab Fermi level and the vacuum energy if the slabs are long enough to avoid the introduction of spurious quantization effects and the influence of the band bending due to pinning of the Fermi level by surface states.

Since we are dealing with metal/dielectric interfaces, the VBO can also be obtained by shifting the planar-averaged total potential in the dielectric region only to locate the dielectric VBE, and taking the difference between the calculated Fermi level and the dielectric VBE. In the PDOS analy-

sis, the VBO can be read directly from the difference between the Fermi level and the top of the dielectric valence band.

To make sure that the calculated VBO's were consistent, we proceeded in the WM method as follows: we took the z average of the planar-averaged total potential between two selected locations in the dielectric and metal (32.4 a.u. and 41.1 a.u./9.6 a.u. and 18.9 a.u. for TiN/SiO₂, and 23.4 a.u. and 32.8 a.u./5.1 a.u. and 10.3 a.u. for TiN/HfO₂, respectively; horizontal bars on wiggled lines in Fig. 4 show the averaged regions), and used those same locations to obtain the z averages for all the structures with modified interfaces. In the case of the PDOS analysis, we projected the density of states onto the Si-O (Hf-O) atoms in the middle of the SiO₂ (HfO₂) slab to infer the approximate location of the VBE for the reference TiN/SiO₂ and TiN/HfO₂ structures (this approach should give the exact location of the VBE for dielectric slabs long enough to avoid the presence of interface states in the projected region). For the remaining interfaces, we projected the DOS onto the same atoms as for the references and compared the PDOS with the corresponding reference to obtain the VBO shift. We also calculated the bulk dielectric band gaps and the PDOS at the interface and first

monolayer in the dielectric to help identify the VBE and CBE (see Fig. 4).

For TiN/SiO₂ the band gap obtained from the PDOS (~ 6.0 eV) is in good agreement with the value from bulk SiO₂ (6.05 eV) using the same basis set (DZP), showing that in this case the SiO₂ slab is thick enough to guarantee bulk properties in its middle. The slight decrease in the band gap may be caused by a residual contribution of interface states below the CBE. As shown in Fig. 4, the DOS projected on the interface O and N atoms displays interface states above the VBE and below the CBE, but while the density of those near-VBE states decreases significantly at the first SiO₂ monolayer away from the interface, the density of near-CBE states remain as intense as at the interface.

For TiN/HfO₂ the agreement between the band gaps obtained from the PDOS at the middle of the HfO₂ slab (~ 3.5 eV) and bulk HfO₂ (3.86 eV) using the same basis set (DZP) is not as favorable as in the TiN/SiO₂ case. Figure 4 shows that like in the previous case the density of interface state decays very quickly near the VBE but remains quite high near the CBE at the first HfO₂ monolayer away from the interface.

These results indicate that the location of the VBE (thus the VBO) is well determined for both systems using the PDOS analysis. On the other hand, with the WM method it is not obvious where to take the average along z of the total potential and different choices lead to VBO's differing by about 200 meV. The difference between the two WM approaches, shifting the planar-averaged potential in the metal and dielectric regions or shifting only in the dielectric and using the VBE/Fermi level difference as the VBO, can be as large as 600 meV and illustrates the uncertainty of the method for short slabs. For example, the WM VBO obtained with the double shift and with the VBE/Fermi level difference for the TiN/SiO₂ and TiN/HfO₂ stoichiometric interfaces are 3.4/2.8 and 3.0/2.4 eV, respectively. Thus, for the structures we have investigated, we attribute a higher degree of confidence to the VBO's obtained using the PDOS technique.

III. RESULTS

A. TiN/SiO₂

Variations of the reference stoichiometric interfaces shown in Fig. 3 were created to study the effect of interface nonstoichiometry and species interdiffusion on the VBO (see Fig. 5).

For the TiN/SiO₂ interface, five cases were considered: (1) replacement of the N rows at the interface by O rows, making all interfacial bonds of the type Ti-O-Si; (2) replacement of the O rows at the interface by N rows, making all the interfacial bonds of the type Ti-N-Si; (3) the stoichiometric interface with 50% Ti-N-Si and 50% Ti-O-Si bonds; (4) removal of the O rows at the interface and reduction of the corresponding Ti-Si distance resulting in an interfacial configuration of approximately 30% Ti-N-Si and 70% Ti-Si bonds; and (5) removal of the O and N rows at the interface and reduction of the TiN-SiO₂ slab distance, resulting in an interfacial configuration of 100% Ti-Si bonds. All cases were

relaxed until the maximum residual force was less than 0.07 eV/Å. Table I summarizes the coordination number in the bulk and interface regions for each case. Some interesting results from this table are the following: (1) For the stoichiometric interface, the coordination numbers are the following: Si 4–5, Ti 4–8, O 3–4, N 3–4. (2) In the 100% O interface, the coordination of Si is much lower than in the bulk, in the 2–3 range, causing the formation of one Si-Ti long bond (2.61 Å, to be compared to less than 2.2 Å for Ti-N and less than 1.7 Å for Si-O in the bulk regions). This is because the interfacial O stays closer to Ti than to Si as demonstrated by the long Si-O interface bonds compared to their bulk values, and contrary to the T-O interface bonds that are of the same length as of bulk Ti-N bonds. (3) In the 100% N interface, all the interfacial Si are fourfold coordinated and do not form bonds to Ti, showing a more balanced distribution of N ions at the interface. (4) For the case with 100% Ti-Si at the interface, one O from the first ML in SiO₂ (-Si-O-Si-Ti-) migrates to the Ti side of the interface and oxidizes it. The resulting SiO₂ near the interface is therefore further reduced with the creation of an O vacancy (Si-Si distance=4.60 Å).

The densities of interface states are highest at or just above the VBE (~ -2.7 eV), in the range -2.7 – -2.0 eV, depending on the interface configuration (see Fig. 6). Other smaller peaks appear just below the CBE (~ 3.3 eV), in the range 2.5–3.3 eV. In the case of partially or fully reduced interfaces other peaks appear throughout the band gap.

Table II summarizes the VBO's obtained for each interface calculated using both the WM and the PDOS (see Fig. 5) methods. The VBO's differ by 600 meV or less using the WM and PDOS methods. This level of disagreement between the two techniques is expected given that the chosen region for taking the z average of the planar-averaged potential in the WM method [Fig. 4(a)] is somewhat arbitrary and the VBO strongly depends on that choice. Despite the different outcomes from the two methods, both show the same trend whereby the VBO increases with the concentration of Ti-Si bonds, varying by 300 meV with respect to the lowest VBO values calculated for O- and N-rich interfaces. This is consistent with experimental data relating an increase in the metal WF_{eff} with oxygen anneals.^{5,6,31} However, experimental data show that the TiN WF_{eff} on SiO₂ is 4.6–4.8 eV (Refs. 4 and 6) from where a VBO of 5.1–5.3 eV can be inferred, a value considerably larger than the theoretical results shown in Table II. We will postpone the discussion of this issue until the next section.

B. TiN/HfO₂

For the case of TiN/HfO₂ interface, seven cases were considered: (1) one-half of the TiN Ti atoms belonging to the closest Ti plane to the interface replaced by Hf atoms; (2) one-third of the HfO₂ Hf atoms belonging to the closest Hf plane to the interface replaced by Ti atoms; (3) one-half of the TiN N atoms belonging to the closest N plane to the interface replaced by O atoms; (4) the stoichiometric interface with 50% Ti-N-Hf and 50% Ti-O-Hf bonds; (5) one-fifth of the interface O atoms replaced by an O vacancy

TABLE I. TiN/SiO₂ and TiN/HfO₂ structural properties: coordination number (the cutoff length for bond counting is 1.1 times the sum of the two covalent radii) and bond length (in eV) in the bulk and interface regions. (\bar{O} = oxygen vacancy.)

Structure	Interface configuration	Coordination number					Bond length (Å)								
		Si	Hf	Ti	O	N	Si-O	Si-N	Si-Ti	Hf-O	Hf-N	Hf-Ti	Ti-O	Ti-N	
bulk SiO ₂		4	—	—	2	—	1.66	—	—	—	—	—	—	—	
bulk HfO ₂		—	7	—	3-4	—	—	—	2.06- 2.27	—	—	—	—		
bulk TiN		—	—	—	6	—	6	—	—	—	—	—	2.06- 2.21		
TiN/SiO ₂ interface	100% Ti-O-Si	2-3	—	5-8	3-4	—	1.74- 1.85	—	2.61	—	—	—	2.00- 2.22	—	
	100% Ti-N-Si	4	—	4-10	—	3-4	—	1.78- 1.88	—	—	—	—	1.91- 2.20		
	50% Ti-O-Si 50% Ti-N-Si	4-5	—	4-8	3-4	3-4	1.78	1.78- 1.98	—	—	—	—	2.11- 2.23	1.95- 2.18	
	30% Ti-N-Si 70% Ti-Si	3	—	4-7	—	3	—	1.87	2.54- 2.61	—	—	—	—	1.95- 2.27	
	100% Ti-Si	3	—	3-7	3	—	—	—	2.41- 2.61	—	—	—	1.98- 2.05	—	
TiN/HfO ₂ interface	50% Ti-N-Hf 50% Ti-O-Hf Hf mixed in TiN	—	5-8	8-10	2-4	3-5	—	—	—	2.18- 2.44	2.17- 2.35	3.04	2.08- 2.24	2.08- 2.23	
	50% Ti-N-Hf 50% Ti-O-Hf Ti mixed in HfO ₂	—	6	4-7	3-4	3-4	—	—	—	1.98- 2.18	2.07- 2.47	—	2.04- 2.17	1.90- 2.19	
	50% Ti-N-Hf 50% Ti-O-Hf O mixed in TiN	—	5-8	5-7	2-3	3-4	—	—	—	2.02- 2.34	2.17- 2.41	3.06	2.08- 2.22	1.93- 2.16	
	50% Ti-N-Hf 50% Ti-O-Hf	—	4-7	5-7	2-4	3-4	—	—	—	2.10- 2.24	2.19- 2.38	—	2.18- 2.20	1.92- 2.23	
	50% Ti-N-Hf 30% Ti-O-Hf	—	5-7	4-6	2-3	3-5	—	—	—	2.19- 2.28	2.11- 2.43	2.95	2.19- 2.24	2.06- 2.20	
	20% Ti- \bar{O} -Hf 100% Ti-Hf	—	3-5	3-5	—	—	—	—	—	—	—	2.98- 3.02	—	—	

(resulting in an O vacancy concentration of 1.2×10^{14} cm⁻²); (6) removal of all interfacial N and O atoms and reduction of the TiN-HfO₂ slab distance, resulting in an interfacial configuration of 100% Ti-Hf bonds. All interface configurations were relaxed until the maximum residual force was less than 0.07 eV/Å. Table I summarizes the coordination number in the bulk and interface regions for each case. Some interesting results from this table are the following: (1) In the stoichiometric case, all interfacial O (coordination number 2-4) bond to both Hf (coordination number 4-7) and Ti (coordination number 5-7) but most N (coordination number 3-4) bond only to Ti. (2) In the case of Hf mixed in TiN, the coordination number of the interfacial Ti ions is rather high, in the range 8-10 (to be compared to 5-7 without Hf mixed in TiN but the same amount of interfacial N and O). The Hf-Ti bond formed in this case is not across the interface but

between the mixed Hf ion and one of its surrounding Ti neighbors. (3) For O mixed in TiN, a Hf-Ti bond 3.06 Å long is formed across the interface. (4) In the case of an O vacancy at the interface, a Hf-Ti bond 2.95 Å long is formed across the interface. (5) For the case of the fully reduced interface (100% Ti-Hf bonds) the coordination number of both Hf (3-5) and Ti (3-5) is rather low and Hf-Ti bonds ~3.0 Å long are formed across the interface.

The densities of TiN/HfO₂ interface states are high at or just above the VBE, in the range -2.4 to -1.7 eV, and at or just below the CBE, in the range 1.0-2.0 eV (see Fig. 6). For the case of Ti mixed in HfO₂ one large peak of Ti-related states appears near the CBE due to the placement of mixed Ti atoms near the interface. For the fully reduced case, a large density of interface states is found throughout the band gap.

TABLE II. TiN/SiO₂ valence band offset (VBO) and effective work function (WF_{eff}) for various interface configurations and calculation techniques (in eV). Direct measurements of the TiN/SiO₂ VBO are not available; however, using Eq. (3) it can be obtained indirectly from capacitance-voltage data (Refs. 4–6) yielding 5.1–5.3 eV.

Interface	100% Ti-O-Si	100% Ti-N-Si	50% Ti-O-Si 50% Ti-N-Si	30% Ti-N-Si 70% Ti-Si	100% Ti-Si
VBO (WM/PDOS)	3.1/2.9	3.1/2.6	3.4/2.8	3.4/2.8	3.4/2.8
WF_{eff} (exp. band gap)	7.0	7.3	7.1	7.1	7.1
WF_{eff} (th. band gap)	4.1	4.4	4.2	4.2	4.2
WF_{eff} (scaled)	5.6	6.0	5.7	5.7	5.7

Table III shows the VBO's for the cases above. The agreement between the WM and PDOS (see Fig. 5) methods for VBO calculation is comparable to that of Ti/SiO₂. Most important, the VBO increases by ~ 1 eV with the decrease of O and/or N at the interface, as in the TiN/SiO₂ case, and in qualitative agreement with experimental data.^{5,6,31} Table III shows that the impact of species interdiffusion on the VBO while keeping the same interface stoichiometry is less important than modifications of the interface stoichiometry itself,

suggesting that sharp interfaces may not be as crucial as the nature of the interfacial bonds in determining the VBO: metal-to-metal or metal-to-Si bonds across the interface mediated by a high-electronegativity atom such as O or N result in a smaller VBO, while interfaces rich in metal-metal or metal-Si bonds result in higher VBO. Similar to the TiN/SiO₂ case, experimental data shows that the TiN WF_{eff}

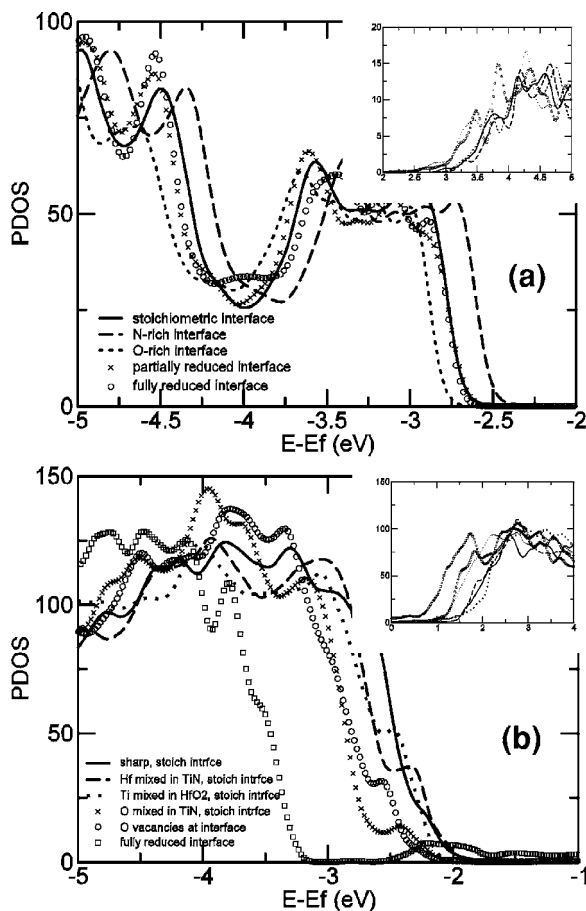


FIG. 5. Valence band edges location as a function of the interface stoichiometry for the (a) TiN/SiO₂ and (b) TiN/HfO₂ interfaces. Insets: same for the conduction band edges.

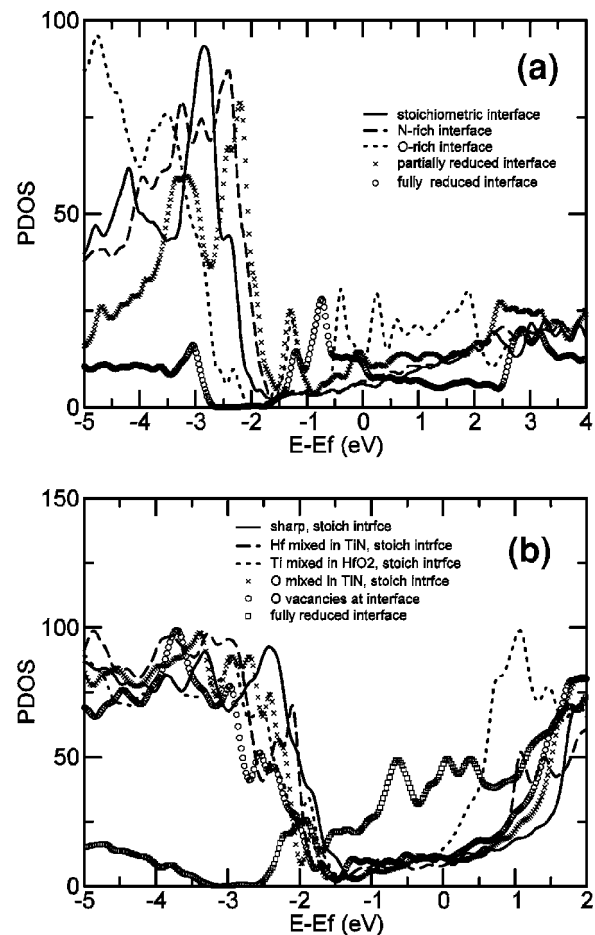


FIG. 6. Projected density of states on the interfacial oxygen and nitrogen atoms plus the (a) first Si monolayer away from the interface for the TiN/SiO₂ system and (b) first Hf monolayer away from the interface for the TiN/HfO₂ system.

TABLE III. TiN/HfO₂ valence band offset (VBO) and effective work function (WF_{eff}) for various interface configurations and calculation techniques (in eV). Direct measurements of the TiN/HfO₂ VBO are not available; however, using Eq. (3) it can be obtained indirectly from capacitance-voltage data (Ref. 4) yielding 3.9 eV. (\bar{O} = oxygen vacancy.)

Interface	50% Ti-N-Hf	50% Ti-N-Hf	50% Ti-N-Hf	50% Ti-N-Hf	50% Ti-N-Hf	50% Ti-N-Hf
	50% Ti-O-Hf	Hf mixed in TiN	50% Ti-O-Hf Ti mixed in HfO ₂	50% Ti-O-Hf O mixed in TiN	50% Ti-N-Hf 30% Ti-O-Hf	20% Ti- \bar{O} -Hf 100% Ti-Hf
VBO (WM/PDOS)	3.0/2.4	4.0/2.5	3.0/2.5	3.0/2.7	3.5/2.7	4.3/3.4
WF_{eff} (exp. band gap)	6.2	6.1	6.1	5.9	5.9	5.2
WF_{eff} (th. band gap)	4.4	4.3	4.3	4.1	4.1	3.4
WF_{eff} (scaled)	5.1	4.9	4.9	4.7	4.7	3.6

on HfO₂ is ~ 4.7 eV (Ref. 4) from where a VBO of ~ 3.9 eV can be inferred, a value larger than all calculated VBO's shown in Table III. We will return to this issue in the next section. To our best knowledge, direct measurements of the TiN/SiO₂ and TiN/HfO₂ VBO's are not available.

The relation between the VBO and the physical nature of the interface bonds can be simply understood in terms of interface dipoles. The presence of the very electronegative O or N atoms between Ti and Hf or Ti and Si pulls electrons from both the metal and the dielectric creating two opposite dipoles. Defining a phenomenological material effective electronegativity EN_{eff} as the geometric average of the Pauling electronegativities EN_i of the N species per formula unit as³²

$$EN_{eff} = \left(\prod_{i=1}^N EN_i \right)^{1/N},$$

we find that the effective HfO₂, SiO₂, and TiN electronegativities are ~ 2.5 , ~ 2.8 , and ~ 2.2 , respectively. Hence, as the TiN EN_{eff} is the smallest of the three, the O-Ti dipole is expected to be larger than the O-Hf and O-Si dipoles resulting in a net negative charge transfer from TiN to the interface O and N atoms and causing the VBO to decrease. In the absence of O at the interface, long Ti-Hf (~ 3.0 Å) and Ti-Si (2.5 – 2.7 Å) bonds or O vacancies form at the interface with negligible charge exchange, increasing the VBO.

IV. EFFECTIVE METAL WORK FUNCTION CALCULATION

In the search for an appropriate metal to replace poly-Si as the gate metal in CMOS technology, the key quantity of interest is the effective work function WF_{eff} , which differs from the vacuum work function WF by the metal/dielectric dipole step (see Fig. 2). Therefore, in order for simulations to serve as a "screening engine" for potential metal gates providing relevant and easily verifiable information in this context, it is highly desirable to be able to determine WF_{eff} from the calculated VBO. The two quantities are trivially related by the expression

$$WF_{eff} = BG_d + EA_d - \text{VBO}, \quad (3)$$

where BG_d and EA_d are the dielectric's band gap and electron affinity. Because the exchange-correlation approximation used in DFT to describe quantum many-body effects results in the underestimation of the band gap, it is necessary to use measured band gaps in the formula above. This approach assumes that the VBO is calculated correctly within the theory used and is standard in studies of band alignment.³⁰ Since measured EA 's are available for SiO₂ [0.9 eV (Ref. 10)] and HfO₂ [2.9 eV (Ref. 12)] those are also used to determine WF_{eff} . The third rows of Tables II and III show the resulting WF_{eff} obtained with this procedure.

Capacitance-voltage (CV) measurements of the TiN WF on SiO₂, which ultimately provide WF_{eff} , give ~ 4.6 eV (Ref. 4) to 4.8 eV (Ref. 5) for plasma vapor deposition (PVD)-grown samples after annealing at 900 °C for the former and 420 °C for the latter. Atomic layer deposition (ALD)-grown TiN on SiO₂ yields 4.8 eV after annealing above ~ 800 °C.⁶ WF_{eff} was also measured for PVD-grown TiN on HfO₂ and it is ~ 4.7 eV after 900 °C anneal.⁴ X-ray diffraction (XRD) analysis of the samples of Ref. 6 indicates no interface reaction for annealing up to 1000 °C and a preferential TiN(111) orientation. As a comparison, we performed calculations of rock-salt TiN(111) using slabs 19 layers thick consisting of alternating Ti and N layers. The calculated WF using GGA is 4.67 eV for a Ti-terminated slab and 7.75 eV for an N-terminated slab. The result for the Ti-terminated slab is in better agreement with the experimental data, indicating that SiO₂ behaves as a quasivacuum for the Ti-terminated TiN surface, and not as a high electronegativity adlayer corresponding to the N-terminated case. Using the usual MIGS formula $WF_{eff} = S(WF - \varphi_{CNL}) + \varphi_{CNL}$ (Ref. 10) for TiN on HfO₂ with $S=0.5$,¹⁰ $\varphi_{CNL}=4.4$ eV below vacuum,^{14,33} $BG(\text{HfO}_2)=5.7$ eV,¹¹ $EA(\text{HfO}_2)=2.9$ eV,¹² and the TiN $WF=4.8$ eV from ALD-grown TiN on SiO₂,⁶ we find that the TiN WF_{eff} on HfO₂ is 4.6 eV. Notice that for data collected under similar experimental conditions in Ref. 4, the TiN WF on HfO₂ is slightly larger than on SiO₂. This is not what is expected from the MIGS model considering

that the HfO₂ CNL is located at ~ 4.4 eV below vacuum.^{14,34} In fact, if this model were to hold for this system, the TiN WF on HfO₂ should be smaller than on SiO₂, as calculated above. This inconsistency is an indication of a strong interface component in the determination of the VBO for this system as discussed in the Introduction.

The available data for the TiN WF_{eff} on SiO₂, which agrees very well with the calculated Ti-terminated TiN vacuum WF , and on HfO₂, which is in reasonable agreement with the MIGS result, is outside the calculated WF_{eff} range of values shown in the third rows of Tables II and III. Since there is no available data mapping in detail the atomic structure at the TiN/dielectric interface, our stoichiometric interface used as the basis for all the other interfaces studied ought to be considered as only a model and should not be expected to reproduce the experimental data with high accuracy. However, even the considerable modifications of the stoichiometric interfaces described in the previous section and summarized in Tables II and III fail to set a range of calculated values which “brackets” the experimental data, especially in the case of SiO₂.

As one more attempt to improve agreement with data, we also calculated WF_{eff} using the theoretical band gaps instead, so that WF_{eff} is derived from calculations only, without any experimental input other than the electron affinities. The fourth rows of Tables II and III show the resulting values, which as before leave the measured TiN WF_{eff} outside the range of the calculated values.

A third approach to calculate WF_{eff} is to compare the TiN/dielectric and dielectric/Si VBO's since ultimately WF_{eff} obtained from CV data is a measure the alignment between the metal Fermi level and the band edges of the Si substrate. Since the calculated TiN/HfO₂ VBO is severely underestimated in our study, perhaps this deficiency can be canceled by a similar problem in the calculation of the Si/HfO₂ VBO. Here we illustrate a technique that takes advantage of such an error cancellation, if it indeed happens. We performed a separate Si/HfO₂ interface calculation¹⁴ with the HfO₂ lattice vectors modified to fit the Si unit cell. Stress caused a decrease of the calculated HfO₂ band gap from 3.86 eV to 3.5 eV. Moreover, the calculated VBO in this case is 3.4 eV, in good agreement with data (3.65 eV) and first-principles calculations (3.5–3.9 eV) of Puthenkovilakam and Chang for the similar Si/ZrO₂ system.³⁴ The MIGS formula for the CBO between dielectrics (1) and (2) is¹⁰

$$\begin{aligned} \text{CBO} = & (EA^{(1)} - \varphi_{CNL}^{(1)}) - (EA^{(2)} - \varphi_{CNL}^{(2)}) \\ & + S(\varphi_{CNL}^{(1)} - \varphi_{CNL}^{(2)}), \end{aligned} \quad (4)$$

where S is the pinning strength of the wider band gap dielectric. Using $EA(\text{Si})=4.0$ eV and $\varphi_{CNL}(\text{Si})=4.9$ eV below vacuum we find $\text{CBO}(\text{Si}/\text{HfO}_2)=0.85$ eV, thus $\text{VBO}(\text{Si}/\text{HfO}_2)=3.75$ eV, in excellent agreement with the data of Ref. 34. In this case we have

$$WF_{eff} = BG_{\text{Si}} + EA_{\text{Si}} + \text{VBO}_{\text{Si-d}} - \text{VBO}_{\text{d-m}}, \quad (5)$$

where d stands for dielectric and m stands for metal. It is easy to see that because the calculated Si/HfO₂ VBO of 3.4 eV is so close to the experimental value of 3.65 eV, this

technique does not improve on the estimation of WF_{eff} . For example, using the calculated TiN/HfO₂ VBO of 2.4 eV for the stoichiometric interface (Table III) the formula above gives $WF_{eff}=6.1$ eV, very close to the result obtained using the experimental band gap technique (third row of Table III).

V. DISCUSSION

Despite the fact that a VBO is the difference between VBE's (or Fermi level/VBE in the case of metal/dielectric) which are ground states of each of the isolated systems forming the interface and therefore are expected to be well described by the DFT/GGA approximation, it is quite clear that a VBO cannot be larger than the widest of the two band gaps at the interface. Since band gaps are underestimated by a factor of about 2, one cannot expect VBO's to be always calculated with great precision. In the case dielectric/dielectric interfaces, the accuracy of calculated VBO's is mixed: 3.1 eV (Ref. 35) (experiment 4.1–4.7 eV) (Refs. 36 and 37) for sharp Si/SiO₂ interfaces but 4.65 eV in the presence of a suboxide;³⁸ for sharp Si/HfO₂ interfaces, it is 3.4 eV (this work; limited by a calculated stressed HfO₂ band gap of 3.5 eV) and 3.5–3.9 eV (Ref. 34) [experiment 3.65 eV (Ref. 34)], just to mention a few examples. However, for the various metal/dielectric interfaces described in this work and for calculations involving different levels of interface oxidation at the metal side of Mo/ZrO₂,³⁹ the agreement with experiment seems rather poor. Because of the band gap underestimation, DFT/GGA calculations limit the VBO's at ~ 5.8 eV and ~ 3.7 eV for SiO₂ and HfO₂, respectively, with some variability depending on the basis set used which impacts the dielectric band gap width. Therefore, our calculated VBO's could be much larger and in fact match experimental data if the limitation in accuracy is determined only by the magnitude of the calculated dielectric band gap.

The possible limitation of DFT/GGA (or DFT/LDA) in predicting correct VBO's is indirectly supported by GW -corrected calculations of the electronic structure of bulk ZrO₂ (Ref. 40) which show that the VBE decreases by approximately 1.2 eV with respect to the DFT result for tetragonal ZrO₂. Therefore the correction of the calculated band gap using the scissors operator (shift of the CBE alone) is incorrect for ZrO₂ and possibly for metal/ZrO₂ interfaces as well since the decrease of the ZrO₂ VBE may not be compensated by a shift of the metal Fermi level under GW . If we assume that the GW correction for the VBE location of bulk monoclinic HfO₂ is the same as for tetragonal ZrO₂ 1.2 eV (Ref. 40) and that the GW shift of the metal Fermi level is negligible, then we obtain $WF_{eff}=5.0$ eV for the stoichiometric interface, in good agreement with data.⁴ However, it is important to realize that while the GW shift of the oxide bulk VBE seems to correct the VBO, this procedure implicitly assumes that the charge transfer across the interface, which adds an energy step to the VBO (obtained in the Schottky limit), is correctly captured within DFT/GGA. If the interface dipole energy is also not accurate, then corrections beyond bulk GW calculations will be necessary.

The self-interaction corrected PP approach (SIC-PP) is, like GW , a step beyond DFT/LDA.⁴¹ We applied SIC-PP to

TABLE IV. Electronic properties of the Mo/HfO₂ interface calculated with the usual DFT/LDA approach and the more sophisticated SIC-PP method. The experimental values for the VBO were obtained from Eq. (3) assuming an electronegativity of 2.9 eV for HfO₂ (Ref. 12).

	LDA	SIC-PP	Experimental
Band gap	3.50	4.95	~5.7 ^a
VBO	1.92	3.44	3.5–3.7
WF_{eff}	6.63	5.11	4.9–5.1 ^b

^aReference 11.

^bReference 43.

calculate the Mo/HfO₂ interface VBO and compared it with the usual DFT/LDA/PP value. We chose Mo instead of TiN in this case because, in addition to the importance and availability of data for Mo, it is a simple metal and not a composite, which reduces the number of SIC-PP's to generate. The optimized geometry of the O-rich Mo/HfO₂ interface was taken from our previous study of Mo/ZrO₂ interfaces.³⁹ A detailed description of the calculation techniques adopted for this system will be published elsewhere. The calculated band gaps, valence band offsets, and effective work functions obtained with the PWSCF code⁴² are shown in Table IV (the VBO's were calculated using the WM method and effective WF 's were calculated using a experimental band gap 5.7 eV and experimental affinity energy 2.9 eV). It is seen that SIC-PP approach not only produces a larger value (closer to experiment) for the HfO₂ band gap, but it also increases the VBO resulting in a smaller WF_{eff} value. Using the SIC-PP approach we obtained a WF_{eff} of 5.1 eV, which is quite close to the measured effective WF_{eff} for Mo on HfO₂ 4.9–5.1 eV (Ref. 43). Thus the SIC-PP method suggests that calculation schemes that improve the band gap value also improve the VBO value. More generally, it suggests that despite being the energy difference between the ground states of two materials the VBO is not a ground state property of the composite system and therefore is not accurately predicted by the DFT/LDA/PP approach.

Besides the fundamental issues described above, we cannot rule out the possibility that further interface modifications may be required to better match the WF data. As indicated by Demkov *et al.*,³⁸ the role played by a graded transition region between the two materials (a suboxide in Si/SiO₂) in the determination of the VBO can be very important and may be the key for a higher VBO, even though high-resolution transmission electron microscopy (HRTEM) and Z-contrast scanning transmission electron microscopy (Z-contrast STEM) images of TiN/HfO₂ samples do not reveal a clear oxide region between the metal and the dielectric for as-deposited or temperature-annealed samples.⁴⁴ However, due to metal/dielectric interface roughness, these characterization techniques cannot completely exclude the possibility of a very thin (less than 10 Å thick) oxide. While further characterization will help understand if a transition region forms at that interface, this scenario could be theoretically explored by more extensive modifications of the model dielectric and metal in the bulk regions close to the interface.

Stress can also be a factor influencing the calculated VBO's, as discussed by Tuttle.³⁵ We noted before that the TiN vacuum WF is not strongly affected by the levels of stress present in the structures, which is an indication but not a proof that the VBO's are also not much affected by stress. A study involving larger unit cells in the lateral direction might be able to answer this question, a proposition that is beyond our current computation capabilities. Another path to investigate this possibility is to vary the unit cell vectors such that stress is distributed more evenly between the oxide and the metal and from there extract trends. A third approach is to compress the HfO₂ and SiO₂ slabs by the TiN lattice vectors. That is the other extreme of stress distribution, in which all the lattice adjustment is taken by the dielectric. We performed such calculations for the stoichiometric interfaces and found that while the HfO₂ and SiO₂ band gaps changed slightly from 3.86 eV and 6.05 eV to 3.82 eV and 6.14 eV, respectively, the TiN/HfO₂ and the TiN/SiO₂ VBO's remained essentially the same. Since in this extreme case the VBO's are unchanged, we can conclude that most likely stress is not the cause of the VBO underestimation.

Finally, the short length of our dielectric and metal slabs are the source of some uncertainty in determining the VBE location from the PDOS and to take meaningful averages of the total potential. Slab calculations indicate that for metal slabs as thick as the ones considered in this work the vacuum WF is within ~50 meV from the converged value, thus the metal slab thickness is not expected to be responsible for the VBO's underestimation. Given that our PDOS plots yield band gaps that are close to bulk calculations, especially for TiN/SiO₂, we do not believe that the large difference between the experimental and theoretical VBO's can be explained by the size of our dielectric slabs. It is conceivable however, that for thicker dielectric slabs a larger amount of charge transfer takes place between the dielectric and the metal causing the Fermi level to shift towards the CBE, increasing the VBO.

Despite all the possible sources of error above, it is surprising that for both TiN/SiO₂ and TiN/HfO₂ interfaces the same trend of large VBO underestimation is observed. Given that SiO₂ and HfO₂ and their interfaces with TiN are so markedly distinct, the results obtained in this work may indicate a general trend in calculations of metal/dielectric VBO's, where the dielectric band gap underestimation limits the calculated VBO magnitude by a scaling factor, distinctively from the dielectric/dielectric interface case where the band gaps set an upper bound to the VBO. At this time we do not have a conclusive explanation why the calculated VBO of dielectric/dielectric interfaces should be treated differently from metal/dielectric interfaces. Further investigation of this matter is ongoing.

VI. CONCLUSIONS

Calculations of the TiN/SiO₂ and TiN/HfO₂ valence band offsets (VBO) were carried out within the DFT/GGA approximation. We found that the presence of O vacancies and Ti-Si or Ti-Hf bonds at the interface cause the VBO to increase. We also considered diffusion of atomic species

across the interface and found that it does not have a large impact on the calculated VBO. The magnitude of the calculated VBO's for both interfaces using the PDOS and the van de Walle-Martin³⁰ techniques is considerably smaller than experiments indicate. Several reasons for such underestimation were analyzed, the most likely being: (i) presence of a transition region several angstroms thick between the dielectric and the metal instead of the sharp interfaces and slight variations considered in this work; (ii) severely reduced metal/dielectric interfaces somewhat different from the ones considered here; (iii) the shortness of our dielectric slabs, which complicates the determination of the VBO's and may limit charge exchange at the interface. Finally we suggest that our metal/dielectric VBO underestimation may not be only due to the details of interface model, but that instead it may be a general feature of such interfaces and scale with the experimental dielectric band gap. Even though a physical picture for this scenario is not available at this time, applying a scaling factor given by the ratio of the experimental to calculated band gaps to our TiN/SiO₂ and TiN/HfO₂ calculated VBO's for stoichiometric or near-stoichiometric interfaces resulted in improved agreement with data.

Finally, the important question whether the high-*K* dielectric HfO₂ with its midrange pinning factor *S* pins the TiN Fermi level cannot be answered in a straightforward way using our results due to the strong dependency of the calculated VBO's on the interfaces' atomic configurations. The lack of experimental information on the detailed interface bonding or even on its average configuration precludes a more judicious choice of candidate interfaces. In addition, a possible limitation of the DFT/GGA approach to calculate accurate valence band offsets between large band gap dielectrics and metals may confine such methodology to qualitative character only.

ACKNOWLEDGMENTS

This work was triggered by experimental data originated at the Motorola's Advanced Process and Research Development Laboratory (APRDL) and compiled by Sri Samavedam and co-workers. We thank them and also Phil Tobin, Bruce White, Chris Hobbs, Jamie Schaeffer, Liang Yong, Rampi Ramprasad, and Alex Demkov for supporting this work and for promoting stimulating discussions.

*Corresponding author. Electronic address: fonseca@vonbraunlabs.com.br

†Electronic address: knizhnik@kintech.ru

¹The International Technology Roadmap for Semiconductors, <http://public.itrs.org>

²*High-k Gate Dielectrics*, edited by M. Houssa (Institute of Physics Publishing, University of Reading, Berkshire, 2004).

³H. J. Hubbard and D. G. Schlom, *J. Mater. Res.* **11**, 2757 (1996).

⁴S. B. Samavedam, L. B. La, P. J. Tobin, B. E. White, C. C. Hobbs, L. R. C. Fonseca, A. A. Demkov, J. Schaeffer, E. Luckowski, A. Martinez, M. Raymond, D. H. Triyoso, D. Roan, V. Dhandapani, R. Garcia, S. G. H. Anderson, K. Moore, H.-H. Tseng, and C. Capasso, *Electron Devices Meeting 2003, IEDM '03 Technical Digest* (IEEE International, Piscataway, NJ, 2003).

⁵G. S. Lujan, T. Schram, L. Pantisano, J. C. Hooker, S. Kubicek, E. Rohr, J. Schuhmacher, O. Kilpelä, H. Sprey, S. D. Gendt, and K. D. Meyer, *Proceedings of the ESSDERC, Firenze, Italy, 2002*, ISBN 88-900847-8-2.

⁶J. Westlinder, T. Schram, L. Pantisano, E. Cartier, A. Kerber, G. S. Lujan, J. Olsson, and G. Groeseneken, *IEEE Electron Device Lett.* **24**, 550 (2003).

⁷B.-Y. Tsui, *IEEE Electron Device Lett.* **24**, 153 (2003).

⁸R. Lin, Q. Lu, P. Ranade, T.-J. King, and C. Hu, *IEEE Electron Device Lett.* **23**, 49 (2002).

⁹I. De, D. Johri, A. Srivastava, and C. M. Osburn, *Solid-State Electron.* **44**, 1077 (2000).

¹⁰J. Robertson, *J. Vac. Sci. Technol. B* **18**, 1785 (2000).

¹¹S. Sayan, E. Garfunkel, and S. Suzer, *Appl. Phys. Lett.* **80**, 2135 (2002).

¹²T. E. Cook, Jr., C. C. Fulton, W. J. Mecouch, R. F. Davis, G. Lucovsky, and R. J. Nemanich, *J. Appl. Phys.* **94**, 7155 (2003).

¹³Y.-C. Yeo, T.-J. King, and Chenming Hu, *J. Appl. Phys.* **92**, 7266 (2002).

¹⁴C. C. Hobbs, L. R. C. Fonseca, A. Knizhnik, V. Dhandapani, S. B. Samavedam, W. J. Taylor, J. M. Grant, L. G. Dip, D. H. Triyoso, R. I. Hegde, D. C. Gilmer, R. Garcia, D. Roan, L. L. Lovejoy, R. S. Rai, E. A. Hebert, H.-H. Tseng, S. G. H. Anderson, B. E. White, and P. J. Tobin, *IEEE Trans. Electron Devices* **51**, 971 (2004); **51**, 978 (2004).

¹⁵S. Lopatin, G. Duscher, T. Liang, W. Windl, G. Lucovski, R. Buczko, S. J. Pennycook, S. T. Pantelides, L. R. C. Fonseca, B. White, C. Fulton, and R. Nemanich, *Phys. Status Solidi B* (to be published).

¹⁶D. M. Ceperley and B. J. Alder, *Phys. Rev. Lett.* **45**, 566 (1980).

¹⁷The same conclusions follow if generalizations of LDA are used instead as they all produce similar band gap values.

¹⁸R. T. Tung, *Phys. Rev. B* **64**, 205310 (2001).

¹⁹H. Hasegawa, Y. Koyama, and T. Hashizume, *Jpn. J. Appl. Phys., Part 1* **38**, 1098 (1999).

²⁰C. Tejedor, F. Flores, and E. Louis, *J. Phys. C* **10**, 2163 (1977).

²¹J. Tersoff, *Phys. Rev. Lett.* **52**, 465 (1984).

²²W. Mönch, *Phys. Rev. Lett.* **58**, 1260 (1987).

²³A. A. Demkov, L. R. C. Fonseca, E. Verret, J. Tomfohr, and O. F. Sankey, *Phys. Rev. B* **71**, 195306 (2005).

²⁴J. P. Perdew and Y. Wang, *Phys. Rev. B* **45**, 13244 (1992).

²⁵P. Hohenberg and W. Kohn, *Phys. Rev.* **136**, B864 (1964).

²⁶W. Kohn and L. J. Sham, *Phys. Rev.* **140**, A1133 (1965).

²⁷J. M. Soler, E. Artacho, J. D. Gale, A. García, J. Junquera, P. Ordejón, and D. Sánchez-Portal, *J. Phys.: Condens. Matter* **14**, 2745 (2002).

²⁸N. Troullier and J. L. Martins, *Phys. Rev. B* **43**, 1993 (1991).

²⁹S. Froyen, *Phys. Rev. B* **39**, 3168 (1989).

³⁰C. G. Van de Walle and Richard M. Martin, *Phys. Rev. B* **35**, 8154 (1987).

³¹J. K. Schaffer, L. R. C. Fonseca, S. B. Samavedam, Y. Liang, P. J. Tobin, and B. E. White, *Appl. Phys. Lett.* **85**, 1826 (2004).

- ³²P. Perfetti, C. Quaresima, C. Coluzza, C. Fortunato, and G. Margaritondo, *Phys. Rev. Lett.* **57**, 2065 (1986).
- ³³A. A. Demkov, L. R. C. Fonseca, J. Tomfohr, and O. F. Sankey, Proceedings of the 2003 MRS Fall Meeting, Boston, 2003 (Materials Research Society, Warrendale, PA).
- ³⁴R. Puthenkovilakam and J. Chang, *Appl. Phys. Lett.* **84**, 1353 (2004).
- ³⁵B. R. Tuttle, *Phys. Rev. B* **67**, 155324 (2003).
- ³⁶H. Nohira, A. Omura, M. Katayama, and T. Hattori, *Appl. Surf. Sci.* **123/124**, 546 (1998).
- ³⁷V. V. Afanas'ev, M. Houssa, and A. Stesman, *Appl. Phys. Lett.* **78**, 3073 (2001).
- ³⁸A. Demkov and O. F. Sankey, *Phys. Rev. Lett.* **83**, 2038 (1999).
- ³⁹A. A. Knizhnik, I. M. Iskandarova, A. A. Bagatur'yants, B. V. Potapkin, and L. R. C. Fonseca, *J. Appl. Phys.* **97**, 064911 (2005).
- ⁴⁰B. Králik, E. K. Chang, and S. G. Louie, *Phys. Rev. B* **57**, 7027 (1998).
- ⁴¹D. Vogel, P. Kruger, and J. Pollmann, *Phys. Rev. B* **54**, 5495 (1996); A. Filippetti and N. A. Spaldin, *Phys. Rev. B* **67**, 125109 (2003).
- ⁴²S. Baroni, A. Dal Corso, S. de Gironcoli, and P. Giannozzi, <http://www.pwscf.org>
- ⁴³Y.-C. Yeo, T.-J. King, and C. Hu, *J. Appl. Phys.* **92**, 7266 (2002).
- ⁴⁴Susanne Stemmer (private communication).